

Turbulent velocity spectra in a quantum fluid: experiments, numerics and theory

Carlo F. Barenghi ^{*}, Victor S. L'vov [†], and Philippe-E. Roche [‡]

^{*}Joint Quantum Centre Durham-Newcastle and School of Mathematics and Statistics, Newcastle University, Newcastle upon Tyne, NE1 7RU, United Kingdom, [†]Weizmann Institute of Science, Dept. Chem. Phys, IL-76100 Rehovot, Israel, and [‡]Univ. Grenoble Alpes / CNRS, Inst NEEL, F-38042 Grenoble, France

Turbulence in superfluid helium is unusual and presents a challenge to fluid dynamicists because it consists of two coupled, interpenetrating turbulent fluids: the first is inviscid with quantised vorticity, the second is viscous with continuous vorticity. Despite this double nature, the observed spectra of the superfluid turbulent velocity at sufficiently large length scales are similar to those of ordinary turbulence. We present experimental, numerical and theoretical results which explain these similarities, and illustrate the limits of our present understanding of superfluid turbulence at smaller scales.

superfluid helium | turbulence | vortex

1. Introduction: motivations.

If cooled below a critical temperature ($T_\lambda \approx 2.18$ K in ^4He and $T_c \approx 10^{-3}$ K in ^3He ¹ at saturated vapour pressure), liquid helium undergoes Bose-Einstein condensation [1], becoming a quantum fluid and demonstrating superfluidity (pure inviscid flow). Besides the lack of viscosity, another major difference from ordinary (classical) fluids such as water or air is that, in helium, vorticity is constrained to vortex line singularities of fixed circulation $\kappa = h/M$, where h is Planck's constant, and M is the mass of the relevant boson ($M = m_4$, the mass of ^4He atom and $M = 2m_3$ the mass of a Cooper pair in ^3He). These vortex lines are essentially one-dimensional space curves, for example, in ^4He the vortex core radius $\xi \approx 10^{-10}$ m is comparable to the inter atomic distance. Thus quantisation of circulation results in the appearance of another characteristic length scale: the mean separation between vortex lines, ℓ . In typical experiments (both in ^4He and ^3He) ℓ is orders of magnitude smaller than the scale D of the largest eddies but is also orders of magnitudes larger than ξ .

There is a growing consensus [2] that superfluid turbulence at large scales $R \gg \ell$ is similar to classical turbulence if excited similarly, for example by a moving grid. The idea is that motions at scales $R \gg \ell$ should involve at least a partial polarization [3, 4, 5] of vortex lines and their organisation into vortex bundles which, at such large scales, should mimic continuous hydrodynamic eddies. Therefore one expects a classical Richardson-Kolmogorov energy cascade, with larger "eddies" breaking into smaller ones. The spectral signature of this classical cascade is indeed observed experimentally in superfluid helium. In the absence of viscosity, in superfluid turbulence the kinetic energy should cascade downscale without loss, until it reaches scales $R \sim \ell$ where the discreteness becomes important. It is also believed that the energy is further transferred downscale by the interacting Kelvin waves (helical perturbation of the individual vortex lines) where it is radiated away by thermal quasi particles (phonons and rotons in ^4He).

Although this scenario seems reasonable, crucial details are yet to be established. Our understanding of superfluid turbulence at scales of the order of ℓ is still at infancy stage, and what happens at scales below ℓ is a question of intensive debates. The "quasi-classical" region of scales, $R \gg \ell$, is better understood, but still less than classical hydrodynamic turbulence. The main reason is that at nonzero temperatures (but still below the critical temperature), superfluid helium is a two-fluid system. According to the theory of Landau and Tisza [6], it consists of two interpenetrating components: the

inviscid superfluid, of density ρ_s and velocity \mathbf{u}_s (associated to the quantum ground state), and the viscous normal fluid, of density ρ_n and velocity \mathbf{u}_n (associated to thermal excitations). The normal fluid carries the entropy and the viscosity of the entire liquid. In the presence of superfluid vortices these two components interact via a mutual friction force[7]. The total helium density $\rho = \rho_s + \rho_n$ is practically temperature independent, while the superfluid fraction ρ_s/ρ is zero at $T = T_\lambda$, but rapidly increases if T is lowered. The normal fluid is essentially negligible below 1K. One would therefore expect classical behaviour only in the high temperature limit $T \rightarrow T_\lambda$, where the normal fluid must energetically dominate the dynamics. Experiments show that this is not the case, thus raising the interesting problem of "double-fluid" turbulence which we review here.

The aim of this article is to present the current state of the art in this intriguing problem, clarify common features of turbulence in classical and quantum fluids, and highlight their differences. To achieve our aim we shall overview and combine experimental, theoretical and numerical results in the simplest possible (and, probably, the most fundamental) case of homogeneous, isotropic turbulence, away from boundaries and maintained in a statistical steady state by continuous mechanical forcing. The natural tools to study homogeneous isotropic turbulence are spectral, thus we shall consider the velocity spectrum (also known as the energy spectrum) and attempt to give a physical explanation for the observed phenomena.

2. Classical vs superfluid turbulence: the background.

We recall [8] that ordinary incompressible ($\nabla \cdot \mathbf{u} = 0$) viscous flow are described by the Navier-Stokes Eq. for the velocity field $\mathbf{u}(\mathbf{r}, t)$

$$\rho[\partial \mathbf{u} / \partial t + (\mathbf{u} \cdot \nabla) \mathbf{u}] = -\nabla p + \mu \nabla^2 \mathbf{u}, \quad [1]$$

where p is pressure, ρ density, μ and $\nu = \mu/\rho$ dynamic and kinematic viscosities. The dimensionless Reynolds number $\text{Re} = VD/\nu$ (where V is the root mean square turbulent velocity fluctuation) estimates the ratio of nonlinear and viscous terms in Eq. [1] at the outer length scale D . In fully developed turbulence ($\text{Re} \gg 1$), D -scale eddies are unstable and give birth to smaller scale eddies, which, being unstable, generate further smaller eddies, and so on. This Richardson-Kolmogorov cascade transfers energy toward viscous scale η , at which the nonlinear and viscous forces in Eq. [1] approximately balance each other; the energy of η -scale eddies is dissipated into heat by viscosity. The hallmark feature of fully developed turbulence is thus the coexistence of eddies of all scales from D to $\eta \simeq D\text{Re}^{-3/4} \ll D$ with universal statistics; the range of length scales $\eta \ll R \ll D$ where both external energy pumping and dissipation can be ignored is called the inertial range.

In isotropic homogeneous turbulence, the energy distribution between scales R is characterized by the one-dimensional energy spectrum $E(k, t)$ with wavenumber $k = 2\pi/R$, normalized such that the energy density (per unit mass) is $E(t) = \frac{1}{V} \int \frac{1}{2} \mathbf{u}^2 dV = \int_0^\infty E(k, t) dk$, where V is volume. In the inviscid limit $E(t)$ is constant, and $E(k, t)$ satisfies the continuity equation

$$\partial E(k, t) / \partial t + \partial \varepsilon(k, t) / \partial k = 0, \quad [2]$$

¹Hereafter by ^3He we mean the B-phase of ^3He

where $\varepsilon(k, t)$ is the energy flux in spectral space. In the stationary case, $E(k, t)$ and $\varepsilon(k, t)$ are t -independent, thus Eq. [2] dictates that the energy flux ε is k -independent. Assuming that this constant ε is the only relevant characteristics of turbulence in the inertial interval and using dimensional reasoning, in 1941 Kolmogorov and Obukhov (KO-41) suggested that the energy spectrum in incompressible, steady, homogeneous, isotropic turbulence in the inertial range is

$$E_{K41}(\varepsilon, k) = C_{K41} \varepsilon^{2/3} k^{-5/3}, \quad C_{K41} \approx 1. \quad [3]$$

This KO-41 $5/3$ law was verified in experiments and numerical simulations of Eq. [1] (up to intermittency corrections discussed below).

In the inviscid limit the energy flux goes to smaller and smaller scales, reaching finally the interatomic scale and accumulating there. To describe this effect, Leith [10] suggested to replace the algebraic relation [3] between $\varepsilon(k)$ and $E(k)$ by the differential form:

$$\varepsilon(k) = -\sqrt{k^{11} E(k)} d[E(k)/8k^2]/dk. \quad [4]$$

This approximation dimensionally coincides with Eq. [3], but the derivative $d[E(k)/k^2]/dk$ guarantees that $\varepsilon(k) = 0$ if $E(k) \propto k^2$. The numerical factor $1/8$, suggested in [11], fits the experimentally observed value of $C_{K41} = (24/11)^{2/3} \approx 1.7$ in Eq. [3].

A generic energy spectrum with a constant energy flux was found in [11] as a solution to the equation $\varepsilon(k) = \varepsilon$ constant:

$$E(\varepsilon, k) = C_{K41} \varepsilon^{2/3} k^{-5/3} [1 + (k/k_{eq})^{11/2}]^{2/3}. \quad [5]$$

Notice that at low k , Eq. [5] coincides with KO-41, while for $k \gg k_{eq}$ it describes a thermalized part of the spectrum, $E(k) \propto k^2$, with equipartition of energy (shown by the solid black line at the right of in Fig. 2A, and, underneath in the same figure, by the solid red line, although the latter occurs in slightly different contexts)².

Although Eq. [3] is the cornerstone of classical turbulence theory, it is only the beginning of the story: in the inertial range the turbulent velocity field is not self-similar, but shows intermittency effects ([8, 9] and references within) which modify the KO-41 scenario.

In this paper we apply these ideas to superfluid helium, explain how to overcome technical difficulties to measure the energy spectrum near absolute zero, and draw the attention to three conceptual differences between classical hydrodynamic turbulence and turbulence in superfluid ^4He .

The first difference is that the quantity which is most easily and frequently detected in helium is not the superfluid velocity but rather the vortex line density \mathcal{L} , defined as the superfluid vortex length per unit volume; in most experiments (and numerical simulations) this volume is the entire cell (or computational box) which contains the helium. This scalar quantity \mathcal{L} has no analogy in classical fluid mechanics and should not be confused with the vorticity, whose spectrum, in the classical KO-41 scenario, scales as $k^{1/3}$ correspondingly to the $k^{-5/3}$ scaling of the velocity. Notice that in a superfluid the vorticity is zero everywhere except on quantized vortex lines. In order to use as much as possible the toolkit of ideas and methods of classical hydrodynamics, we shall define in the next sections an "effective" superfluid vorticity field ω_s . This definition (which indeed [12] yields the classical $k^{1/3}$ vorticity scaling) is possible on scales $R \gg \ell$, provided that the vortex lines contained in a fluid parcel are sufficiently polarized. This procedure opens the way for a possible identification of "local" values of $\mathcal{L}(r, t)$ with the magnitude $|\omega_s|$ of the vector field ω_s .

The second difference is that liquid helium below T_λ is a two fluid system, and (in ^4He) we expect *both* superfluid and normal fluid to be turbulent. This makes superfluid turbulence much richer than classical turbulence, but the analysis becomes more involved, as mutual friction between normal and superfluid components leads to (dissipative) energy exchange between them in either direction.

The third difference is the existence of the intermediate scale ℓ which makes it impossible to apply arguments of scale invariance to the entire inertial interval and calls for its separation into three ranges. The first is a "hydrodynamic" region of scales $\ell \ll R \ll D$ (corresponding to $k_D \ll k \ll k_\ell$ in k -space where $k_D = 2\pi/D$ and $k_\ell = 2\pi/\ell$), which is similar (but not equal) to the classical inertial range; the second is a "Kelvin wave region" $\xi \ll R \ll \ell$ where energy is transferred further to smaller scales³ by interacting Kelvin waves. In the third, less understood intermediate region $R \approx \ell$, the energy flux is caused probably by vortex reconnections.

3. Experiments: flows, probes and spectra.

In this section we shall limit⁴ our discussion to experimental techniques for ^4He . Possibly the simplest way to generate turbulence in ^4He is the application of a temperature gradient which creates a flow of the normal component carrying heat from the hot to the cold plate; this flow is compensated by the counterflow of the superfluid component in the opposite direction which maintains a zero mass flux. This form of heat conduction, called thermal counterflow, is unlike what happens in ordinary fluids. Moreover, under thermal drive, the energy pumping is dominated by the intervortex length scale ℓ and according to numerical simulations there is no inertial interval in which the energy flux scales over the wavenumbers as in the KO-41 scenario [15]. This "quantum" superfluid turbulence [16] is thus very different from classical developed turbulence and will not be discussed here.

From the experimental viewpoint, mechanical generation of turbulence (more similar to what is done in the study of ordinary turbulence) is not as straightforward. Nevertheless, there is a number of successful approaches, which can be classified into three categories: (i) flows driven by vibrating objects, (ii) one-shot-flows driven by single-stroke-bellows, towed grids or spin-up/down of the container, and (iii) flows continuously driven by propellers. Most efforts in characterising turbulent fluctuations have focused on the third category – which allows to produce flows with better homogeneity and isotropy than those generated by vibrating objects, and allows better statistical convergence (and improved stationarity) than measurements in non-stationary flows.

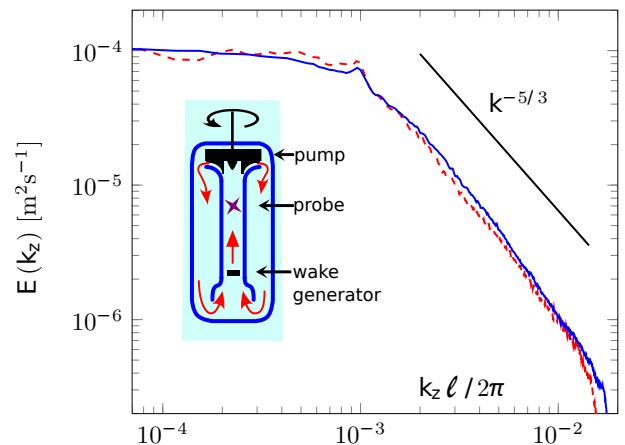


Fig. 1: Color online. Energy spectrum measured in the TOUPIE wind-tunnel (inset) below the superfluid transition (solid blue line, $1.56 \text{ K} < T_\lambda$) and above T_λ (dashed red line) [20].

² In the simulations shown in Fig. 2A, the energy flux $\varepsilon(k)$ is not preserved along the cascade, but continuously decreases due to dissipation and ultimately vanishes at the maximum k .

³ Actually phonon emission will terminate the Kelvin cascade at scales $R \sim 100\xi$ in ^4He [13].

⁴ The methods used in ^3He , at temperatures one thousand times smaller, are rather different [14], and we shall only cite the results in ^3He which are directly relevant to our aim

The quantum phase of ^4He (called He-II) is created by cooling the classical phase (called He-I) below T_λ , thus in most cases the same apparatus or technique can be used to probe classical and quantum turbulence, which helps making comparisons. Three flow configurations have been explored (see also Fig. 3 in the Appendix). Von Karman flows driven by counter-rotating propellers using cryogenic [17] or room temperature [18, 19] motors. Wind-tunnels (see inset in Fig. 1) [21, 20] pressurised hydrostatically by a column of liquid ^4He to allow cavitation-free operation in He-I (in He-II, cavitation is prevented by the fluid high thermal conductivity). Without pressurisation, bubbles would form in He-I preventing the comparison of turbulence above and below T_λ in the same apparatus. The third configuration – the TSF circulator – consists of a pressurised helium loop cooled by a heat exchanger [22]. All these flows are driven by the centrifugal force generated by propellers; not depending on viscous or thermal effects, this forcing is well fitted to liquid helium, irrespectively of its superfluid density fraction.

Probing cryogenic flows is often more challenging than producing the flow themselves: dedicated probes often have to be designed and manufactured for each experiment, and good space and time resolutions are needed to resolve the fluctuating scales of superfluid turbulence ([17, 22, 20, 91], see also Fig. 4 in the Appendix). Below T_λ , the most commonly-used local velocity probe is based on the principle of the ‘‘Pitot’’ (or ‘‘Prandtl’’ or ‘‘total head pressure’’) tube. One end of a tube is inserted parallel to the mean flow, while the other end is blocked by a pressure gauge. The stagnation point which forms at the open end of the tube is associated with an overpressure P probed by the gauge, which is related to the incoming flow velocity V via Bernoulli relation $P \simeq \rho V^2/2$ (hence fluctuations δP of P are proportional to fluctuations δV of V up to terms of the order of $(\delta V/V)^2$). The operation and limitations of such stagnation-pressure probes T_λ are discussed in Ref. [22] (in particular excessive angles of attack lead to measurement bias). Pitot tubes achieving nearly 0.5-mm spatial resolution, and others with DC-4 kHz bandwidth have been operated successfully. At such scales and in the turbulent flows of interest, helium’s two components are expected to be locked together – as discussed later – and described by a single fluid of total density ρ , thus stagnation pressure probes determine their the common velocity.

The first experimental turbulent energy spectra below T_λ were reported in 1998 [17] (using the set-up illustrated at the left of Fig. 3 in the Appendix). Energy spectra at 2.08 K and 1.4 K were found very similar to the spectrum measured in He-I at 2.3 K. In the range of frequencies corresponding to the length scale of the forcing and the smallest resolved length scale, the measured spectrum was compatible with KO-41. The next published confirmation of KO-41 came in 2010 [22] from two independent experiments (of the two types depicted at the centre and at the right of Fig. 3). Measurements obtained with the first type of wind-tunnel are reproduced in Fig. 5, which shows energy spectra at 1.6 K for various mean velocities of the flow. We note that four decades separate the integral scale of the flow ($D \simeq 10$ mm) and the intervortex scale $\ell \simeq 1\mu\text{m}$, to be compared with the 1 mm effective resolution of the anemometer. Measurements obtained with the second type of wind-tunnel explored grid turbulence. Although the signal-to-noise ratio was not as good (see [22] for compensated energy spectra), the choice of a well-defined homogeneous isotropic flow allowed to measure the dissipation rate ε from the spatial decay of kinetic energy behind the grid. The Kolmogorov constant C_{K41} derived from Eq. [3] was found similar above the superfluid transition and below it in He-II at $T = 2.0\text{K}$. The energy spectrum shown in Fig. 1 has been recently obtained in the TOUPIE wind-tunnel both above and below T_λ in the far wake of a disc⁵. A one-to-one comparison of both datasets allowed to check the validity of the $-4/5$ Karman-Howarth law [20] below T_λ ; this law, sometimes described as the only exact relation known in turbulence, confirms that energy cascades from large to small scales with-

out dissipation within the inertial range where the KO-41 scaling is observed.

4. Equations of motion: three levels of description.

In the absence of superfluid vortices, Landau’s two-fluid equations[6] for the superfluid and normal fluid velocities \mathbf{u}_s and \mathbf{u}_n account for all phenomena observed in He-II at low velocities, for example second sound and thermal counterflow. In the incompressible limit ($\nabla \cdot \mathbf{u}_s = 0, \nabla \cdot \mathbf{u}_n = 0$) Landau’s equations are:

$$\rho_s [(\partial \mathbf{u}_s / \partial t) + (\mathbf{u}_s \cdot \nabla) \mathbf{u}_s] = -\nabla p_s, \quad [6a]$$

$$\rho_n [(\partial \mathbf{u}_n / \partial t) + (\mathbf{u}_n \cdot \nabla) \mathbf{u}_n] = -\nabla p_n + \mu \nabla^2 \mathbf{u}_n, \quad [6b]$$

where the efficient pressures p_s and p_n are defined by $\nabla p_s = (\rho_s/\rho) \nabla p - \rho_s S \nabla T$ and $\nabla p_n = (\rho_n/\rho) \nabla p + \rho_s S \nabla T$ (T and S are temperature and entropy). On physical ground, Landau argued that the superfluid is irrotational.

The main difficulty in developing a theory of superfluid turbulence is the lack of an established set of equations of motion for He-II in the presence of superfluid vortices. We have only models at different levels of description.

4A. First level. At the most microscopic level of description, we must account for phenomena at the length scale of the superfluid vortex core, $R \approx \xi$. Monte Carlo models of the vortex core [23], although realistic, are not suitable for the study of the dynamics and turbulent motion. A practical model of a pure superfluid is the Gross-Pitaevskii Equation (GPE) for a weakly-interacting Bose gas [1]:

$$i\hbar \frac{\partial \Psi}{\partial t} = -\frac{\hbar^2}{2M} \nabla^2 \Psi + V_0 |\Psi|^2 \Psi - E_0 \Psi, \quad [7]$$

where $\Psi(\mathbf{r}, t)$ is the condensate’s complex wave function, V_0 the strength of the interaction between bosons, E_0 the chemical potential and M the boson mass. The condensate’s density $\tilde{\rho}_s$ and velocity $\tilde{\mathbf{v}}_s$ are related to $\Psi = |\Psi| \exp(i\Theta)$ via the Madelung transformation $\tilde{\rho}_s = M |\Psi|^2$, $\tilde{\mathbf{u}}_s = \hbar \nabla \Theta / M$, which confirms Landau’s intuition that the superfluid is irrotational. It can be shown that, at length scales $R \gg \xi = \hbar / \sqrt{2ME_0}$, the GPE reduces to the classical continuity equation and the (compressible) Euler equation. It must be stressed that, although the GPE accounts for quantum vortices, finite vortex core size (of the order of ξ), vortex nucleation, vortex reconnections, sound emission by accelerating vortices and Kelvin waves, it is only a qualitative model of the superfluid component. He-II is a liquid, not a weakly-interacting gas, and the condensate is only a fraction of the superfluid density ρ_s . No adjustment of V_0 and E_0 can fit both the sound speed and the vortex core radius, and the dispersion relation of the uniform solution of Eq. [7] lacks the roton’s minimum which is characteristic of He-II [6, 24]. Strictly speaking, we cannot identify $\tilde{\rho}_s$ with ρ_s and $\tilde{\mathbf{u}}_s$ with \mathbf{u}_s . Nevertheless, when solved numerically, the GPE is a useful model of superfluid turbulence at low T where the normal fluid fraction vanishes, and yields results which can be compared to experiments, as we shall see.

4B. Second level. Far away from the vortex core at length scales $R \gg \xi$, and in the zero Mach number limit, the GPE describes incompressible Euler dynamics. This is the level of description of the Vortex Filament Model (VFM) of Schwarz [25]. The nature of the vortex core is ignored and individual vortex lines are described as oriented space curves $\mathbf{s}(\zeta, t)$ of infinitesimal thickness and circula-

⁵ To normalise the x-axis of this plot, the mean intervortex distance ℓ in He-II was estimated using the relation $2\ell/D = \text{Re}_\kappa^{-3/4}$ [56] where $\text{Re}_\kappa = DV/\kappa$ is a Reynolds number defined using the root mean square velocity from the anemometer, and the prefactor 2 was fitted to experimental and numerical data in the range $T \simeq 1.4 - 1.6$ K.

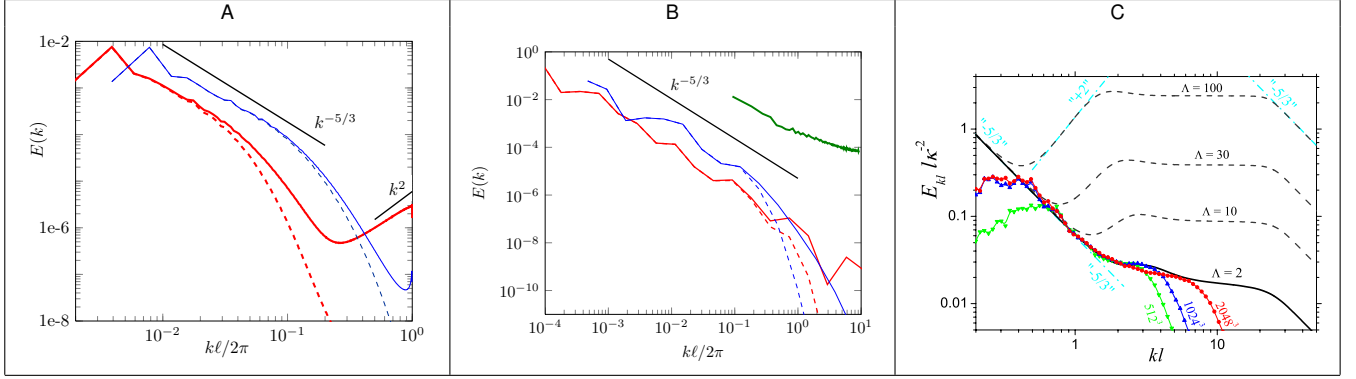


Fig. 2: Color online. Numerical energy spectra $E_s(k\ell)$ (resp. $E_n(k\ell)$) of the superfluid (resp. normal) component for three levels of descriptions by Eqs. [9], [8] and [7]: Panel A: $E_s(k\ell)$ (solid line) and $E_n(k\ell)$ (dashed line) spectra from DNS of the HVBK Eqs. [9] at $T \simeq 1.15\text{K}$ (red) and $\simeq 2.157\text{K}$ (blue) with truncation of phase space beyond the intervortex scale [20]. Panel B: $E_s(k\ell)$ from VFM simulations [8] at $T = 2.164\text{K}$ (solid green line) [83] with synthetic turbulence prescribed for the normal component. $E_s(k\ell)$ (red/blue solid line) and $E_n(k\ell)$ (red/blue dashed line) spectra from shell model simulation of the HVBK equations at 1.44 K (red) and 2.157 K (blue) [58]. Panel C: $E_s(k\ell)$ from GPE simulations [7][40]. The numerical resolution is 2048^3 (red line), 1024^3 (dashed blue line) and 512^3 (green dots). The intervortex distance ℓ results from a fit of the data (see original publication). In all panels, the normalisation of the x-axis (wavevector k) highlights the mean intervortex distance ℓ . Black dashed lines show analytical predictions of the bottleneck [92] discussed in Sec. 6C with different $\Lambda = \ln(\ell/\xi)$. The black solid line with $\Lambda = 2$ corresponds to the simulation in Ref. [40]. The dashed cyan lines show (from the left) the KO-41 $(-5/3)$ scaling, the energy equipartition scaling $(+2)$ and, at the right, the $(-5/3)$ Kelvin wave LN spectrum.

tion κ , where ζ is the arc length, which evolve according to

$$\frac{d\mathbf{s}}{dt} = \mathbf{u}_{\text{si}} + \mathbf{w}, \quad \mathbf{u}_{\text{si}}(\mathbf{s}) = \frac{\kappa}{4\pi} \oint_{\mathcal{L}} \frac{(\mathbf{s}_1 - \mathbf{s}) \times d\mathbf{s}_1}{|\mathbf{s}_1 - \mathbf{s}|^3}, \quad [8a]$$

$$\mathbf{w} = \alpha \mathbf{s}' \times \mathbf{u}_{\text{ns}} - \alpha' \mathbf{s}' \times [\mathbf{s}' \times \mathbf{u}_{\text{ns}}], \quad \mathbf{u}_{\text{ns}} = \mathbf{u}_n - \mathbf{u}_{\text{si}}. [8b]$$

Here the self-induced velocity \mathbf{u}_{si} is given by the Biot-Savart law [26], and the line integral extends over the vortex configuration. At nonzero temperatures the term \mathbf{w} accounts for the friction between the vortex lines and the normal fluid [7]. The unit tangent at \mathbf{s} is $\mathbf{s}' = d\mathbf{s}/d\zeta$, and α, α' are known temperature-dependent friction coefficients. In the $T \rightarrow 0$ limit, α and α' are negligible [27], and we recover the classical result that each point of the vortex line is swept by the velocity field produced by the entire vortex configuration.

Numerical simulations require the discretization of vortex lines in a Lagrangian fashion and the desingularization of Biot-Savart integrals; reconnections are additional algorithmic *ad-hoc* procedures that change the way pairs of discretization points are connected. Reconnection criteria are described and discussed in Ref. [28, 29]; Ref. [30] compares GPE and VFM reconnections with each other and with experiments. Simulations at large values of vortex line density are performed using a tree algorithm [28] which speeds up the evaluations of Biot-Savart integrals from N^2 to $N \log N$ where N is the number of discretization points. The major drawback of the VFM is that the normal fluid \mathbf{u}_n is imposed (either laminar or turbulent), therefore the back-reaction of the vortex lines on \mathbf{u}_n is not taken into account. The reason is the computational difficulty: a self-consistent simulation would require the simultaneous integration in time of Eq. [8] for the superfluid, and of Eq. [1] for the normal fluid, complemented with suitable friction forcing at vortex lines singularities and restoring the momentum balance associated with mutual friction. Such self-consistent simulations were carried out only for a single vortex ring [31] and for the initial growth of a vortex cloud [32]. This limitation is likely to be particularly important at low and intermediate temperatures (at high temperatures the normal fluid contains most of the kinetic energy, so it is less likely to be affected by the vortices).

4C. Third level. At the third level of description we do not distinguish individual vortex lines any longer, but rather consider fluid parcels

which contain a continuum of vortices. At these length scales $R \gg \ell$ we seek to generalise Landau's equations [6] to the presence of vortices. In laminar flows, the vortex lines (although curved) remain locally parallel to each other, so it is possible to define the components of a macroscopic vorticity field $\boldsymbol{\omega}_s$ by taking a small volume larger than ℓ and considering the superfluid circulation in the planes parallel to the Cartesian directions (alternatively, the sum of the oriented vortex lengths in each Cartesian direction). We obtain the so-called Hall-Vinen (or HVBK) "coarse-grained" equations [33, 34]:

$$\rho_s [\partial \mathbf{u}_s / \partial t + (\mathbf{u}_s \cdot \nabla) \mathbf{u}_s] = -\nabla p_s - \rho_s \mathbf{f}_{\text{ns}}, \quad [9a]$$

$$\rho_n [\partial \mathbf{u}_n / \partial t + (\mathbf{u}_n \cdot \nabla) \mathbf{u}_n] = -\nabla p_n + \mu \nabla^2 \mathbf{u}_n + \rho_s \mathbf{f}_{\text{ns}}, \quad [9b]$$

$$\mathbf{f}_{\text{ns}} = \alpha \hat{\boldsymbol{\omega}}_s \times (\boldsymbol{\omega}_s \times \mathbf{u}_{\text{ns}}) + \alpha' \hat{\boldsymbol{\omega}}_s \times \mathbf{u}_{\text{ns}}, \quad [9c]$$

where $\boldsymbol{\omega}_s = \nabla \times \mathbf{u}_s$, $\hat{\boldsymbol{\omega}}_s = \boldsymbol{\omega}_s / |\boldsymbol{\omega}_s|$, and \mathbf{f}_{ns} is the mutual friction force⁶. The difficulty with applying the HVBK equations to turbulence is that in turbulent flows the vortex lines tend to be randomly oriented with respect to each other, so the components of \mathbf{s}' partially or totally cancel out to zero, resulting in local vortex length (hence energy dissipation) without any effective superfluid vorticity. In this case, the HVBK equations may become a poor approximation and underestimate the mutual friction coupling. Nevertheless, they are a useful model of large scale superfluid motion with characteristic scale $R \gg \ell$, particularly because (unlike the VFM) they are dynamically self-consistent (normal fluid and superfluid affect each other). We must keep in mind that Eq. [9] do not have physical meaning at length scales smaller than ℓ . In the literature the mutual friction force is often simplified to $\mathbf{f}_{\text{ns}} = -\alpha \kappa \mathcal{L} \mathbf{u}_{\text{ns}}$ where $\mathcal{L} = 1/\ell^2$.

⁶Strictly speaking, the right hand side of the superfluid equation contains also the vortex tension force $\nu_s \boldsymbol{\omega}_s \times (\nabla \times \hat{\boldsymbol{\omega}}_s)$ where $\nu_s = \kappa / (4\pi) \ln(\ell/\xi)$. This term is essential when describing fully polarized flows, such as Taylor-Couette flow [35, 36] and helical vortex fronts [37]: In these flows, the vortex lines are fully polarised and aligned in the same direction, and their density and orientation may change locally and vary as a function of position (on length scales $R \gg \ell$). However, the vortex tension force is small at high velocity and conserves energy, so it is ignored in the study of turbulence.

⁷De Waele and collaborators used solid boundary conditions [46] and investigated flat and a parabolic normal fluid profiles, an issue which is still open.

5. Numerical experiments: GPE, VFM and HVBK.

Since the pioneering work of Schwarz [25], numerical experiments have played an important role, allowing the exploration of the consequences of limited sets of physical assumptions in a controlled way, and providing some flow visualization.

5A. The GPE. Numerical simulations of the GPE in a three-dimensional periodic box have been performed for decaying turbulence [38] following an imposed arbitrary initial condition, and for forced turbulence [39, 40]. Since the GPE allows sound waves, in order to analyse turbulent vortex lines, it is necessary to extract from the total energy of the system (which is conserved during the evolution) the incompressible kinetic energy part whose spectrum is relevant to our discussion. To reach a steady state, large-scale external forcing and small-scale damping was added to the GPE [40]. The resulting turbulent energy spectrum agrees with KO–41 scaling in homogeneous (see Fig. 2, cyan dot-dashed line) and demonstrates bottleneck energy accumulation near the intervortex scale at zero temperature predicted earlier in [92] and discussed in the Sect. 6C. The KO–41 scaling observed in GPE simulations was found to be consistent with the VFM at zero temperature [51, 12] and has also been observed when modelling a trapped atomic Bose–Einstein condensate [41].

The GPE can be extended to finite temperatures [42, 43, 44] accounting for mutual friction [45].

5B. The VFM. Most VFM calculations have been performed in a cubic box of size D with periodic boundary conditions⁷. At $T \neq 0$ we expect that the normal fluid is turbulent because its Reynolds number $Re = DV_n/\nu_n$ is large (where V_n the root mean square normal fluid velocity). Recent VFM studies thus assumed the form [15, 47, 5]

$$\mathbf{u}_n(\mathbf{s}, t) = \sum_{m=1}^M (\mathbf{A}_m \times \mathbf{k}_m \cos \phi_m + \mathbf{B}_m \times \mathbf{k}_m \sin \phi_m),$$

where $\phi_m = \mathbf{k}_m \cdot \mathbf{s} + f_m t$, \mathbf{k}_m and $f_m = \sqrt{k_m^3 E(k_m)}$ are wave vectors and angular frequencies. The random parameters \mathbf{A}_m , \mathbf{B}_m and \mathbf{k}_m are chosen so that the normal fluid's energy spectrum obeys KO–41 scaling $E(k_m) \propto k_m^{-5/3}$ in the inertial range $k_D \simeq k_1 < k < k_M \simeq k_\ell$. This synthetic turbulent flow [48] is solenoidal, time-dependent, and compares well with Lagrangian statistics obtained in experiments and direct numerical simulations of the Navier-Stokes equation. Other VFM models included normal-fluid turbulence generated by the Navier–Stokes equation [49] and a vortex-tube model [50], but, due to limited computational resources, only a snapshot of the normal fluid, frozen in time, was used to drive the superfluid vortices.

In all numerical experiments, after a transient from some initial condition, a statistical steady state of superfluid turbulence is achieved, in the form of a vortex tangle in which $\mathcal{L}(t)$ fluctuates about an average value independent of the initial condition. It is found [15, 47, 5] that the resulting superfluid energy spectrum $E_s(k)$ is consistent with KO–41 scaling in the hydrodynamic range $k_D < k < k_\ell$ (see the green line of Fig. 2B). This result holds true at zero temperature, where $\rho_n = 0$ [51, 12], in agreement with the GPE.

Recent analytical [4] and numerical studies [15, 5] of the geometry of the vortex tangle reveal that the vortices are not randomly distributed, but there is a tendency to locally form bundles of co-rotating vortices, which keep forming, vanish and reform somewhere else. These bundles associate with the Kolmogorov spectrum: if turbulence is driven by a uniform normal fluid (as in the original work of Schwarz [25]⁸), there are no Kolmogorov scaling nor bundles. Bagaley et al. [5] decomposed the vortex tangle in a polarised part (of density L_\parallel) and a random part (of density L_\times), as argued by Roche & Barenghi [53], and discovered that L_\parallel is responsible for the $k^{-5/3}$ scaling of the energy spectrum, and L_\times for the $f^{-5/3}$ scaling of the vortex line density fluctuations, as suggested in Ref. [21].

5C. The HVBK equations. From a computational viewpoint, the HVBK equations are similar to the Navier-Stokes equation [1]. Not surprisingly, standard methods of classical turbulence have been adapted to the HVBK equations, e.g. Large Eddy Simulations [54], Direct Numerical Simulations [55, 56] and Eddy Damped Quasi-Normal Markovian simulations [57].

The HVBK equations are ideal to study the coupled dynamics of superfluid and normal fluid in the limit of intense turbulence at finite temperature. Indeed, by ignoring the details of individual vortices and their fast dynamics, HVBK simulations do not suffer as much as VFM and GPE simulations from the wide separation of space and time scales which characterize superfluid turbulence. Moreover, well optimized numerical solvers have been developed for Navier-Stokes turbulence and they can be easily adapted to the HVBK model. Simulations over a wide temperature range ($1.44 < T < 2.157$ K corresponding to $0.1 \leq \rho_n/\rho_s \leq 10$) show evidence of strong locking of superfluid and normal fluid ($\mathbf{u}_s \approx \mathbf{u}_n$) at large scales, over one decade of inertial range ([55]). In particular, it was found that even if one single fluid is forced at large scale (the dominant one), both fluids still get locked very efficiently. Fig. 2A illustrates velocity spectra generated by direct numerical simulation of the HVBK equations. A clear $k^{-5/3}$ spectrum is found for both fluid components, at all temperature and large scales.

We have said that the HVBK equations are valid only for $R \gg \ell$. In order to tackle the difficult intermediate regime $R \approx \ell$, a quantum constraint can be re-introduced in this model by truncating superfluid phase space for $|\mathbf{k}| \leq \ell^{-1}$, causing an upward trend of the low temperature velocity spectrum of Fig. 2A which can be interpreted as partial thermalization of superfluid excitations. This procedure also leads to the prediction $\mathcal{L}D^2 = 4Re^{3/2}$ [56] which is consistent with experiments and allows to identify the spectrum of $\mathcal{L}(r)/\kappa$ with the spectrum of the scalar field $|\omega_s(r)|$.

Essential simplification of the HVBK Eqs. [9] can be achieved with the shell-model approximation [58, 59, 60]. The complex shell velocities $u_m^s(k_m)$ and $u_m^n(k_m)$ mimic the statistical behaviour of the Fourier components of the turbulent superfluid and normal fluid velocities at wavenumber k . The resulting ordinary differential Eqs. for $u_m^{n,s}$ capture important aspects of the HVBK Eqs. [9], including the relation between Re and \mathcal{L} . The red and blue solid lines of Fig. 2B show spectra obtained using a shell model. Because of the geometrical spacing of the shells ($k_m = 2^m k_0$), this approach allows more decades of k -space than Eqns. [9] (eight decades in k -space in Ref. [60]). This extended inertial range allows detailed comparison of intermittency effects in superfluid turbulence and classical turbulence.

6. Theory

In this section we discuss our theoretical understanding of superfluid turbulence, moving from the better understood to the less understood case.

6A. Hydrodynamic regime. Large scale ($R \gg \ell$) motions in ^4He at $k \ll k_\ell$ are understood on the ground of the HVBK Eqs. [9]. The simpler, pedagogical case of ^3He (in which the normal fluid is essentially clamped to the walls due to its large viscosity) is discussed in the Appendix [61, 60]. In the case of two coupled fluids, the HVBK Eqs. [9] result in a system of energy balance equations for superfluid and normal fluid energy spectra $E_s(k)$ and $E_n(k)$ [62]:

$$\frac{d\varepsilon_s(k)}{dk} + \Gamma [E_s(k) - E_{ns}(k)] = 0, \quad [10a]$$

$$\frac{d\varepsilon_n(k)}{dk} + \frac{\rho_s}{\rho_n} \Gamma [E_n(k) - E_{ns}(k)] = -2\nu_n k^2 E_n(k). \quad [10b]$$

⁸recently tested in Ref. [52].

Here we approximate Eq. [9c] as $\mathbf{f}_{\text{ns}} - \Gamma \mathbf{u}_{\text{ns}}$, with $\Gamma = \alpha \kappa \omega_{\text{T}}$, $\omega_{\text{T}} \equiv \sqrt{\langle |\boldsymbol{\omega}_s|^2 \rangle}$ is the characteristic ‘‘turbulent’’ superfluid vorticity, estimated by $\langle |\boldsymbol{\omega}_s|^2 \rangle \approx 2 \int_{k_0}^{1/\ell} k^2 E(k) dk$. Superfluid and normal fluid energy fluxes $\varepsilon_s(k)$ and $\varepsilon_n(k)$ can be expressed via $E_s(k)$ and $E_n(k)$ by differential closure [4]. The cross-correlation function $E_{\text{ns}}(k)$ is normalized such that $\int E_{\text{ns}}(k) dk = \langle \mathbf{u}_s \cdot \mathbf{u}_n \rangle$. If, at given k , superfluid and normal fluid eddies are fully correlated (locked), then $E_{\text{ns}}(k) = E_s(k) = E_n(k)$. If they are statistically independent (unlocked), then $E_{\text{ns}}(k) = 0$. The following closure equation for $E_{\text{ns}}(k)$ has been proposed [62]:

$$E_{\text{sn}}(k) = \frac{\rho_s E_s(k) + \rho_n E_n(k)}{\rho [1 + K(k)]}, \quad K(k) \equiv \frac{\rho_n [\nu_n k^2 + \gamma_n(k) + \gamma_s(k)]}{\rho \alpha \omega_{\text{T}}} \quad [10c]$$

Here $\gamma_n(k) \simeq k \sqrt{k E_n(k)}$ and $\gamma_s(k) \simeq k \sqrt{k E_s(k)}$ are characteristic turnover frequencies of eddies in the normal and superfluid components. They are related to the effective turbulent viscosity ν_{T} by $\nu_{\text{T}} k^2 = \gamma(k)$.

For large mutual friction or/and small k of interest in this section, $K(k) \ll 1$, and Eq. [10c] has the physically motivated solution $E_{\text{sn}}(k) = E_s(k) = E_n(k)$ corresponding to full locking $\mathbf{u}_n(\mathbf{r}, t) = \mathbf{u}_s(\mathbf{r}, t)$. In this case the sum of Eq. [9a] (multiplied by ρ_s) and Eq. [9b] (multiplied by ρ_n) yields the Navier-Stokes equation with effective viscosity $\tilde{\nu} = \mu/\rho$. Thus, in this region of k -space, one expects classical behaviour of hydrodynamic turbulence with KO–41 scaling [3] (up to intermittency corrections discussed in Sec. 6C).

6B. Kelvin wave regime. The range $R \ll \ell$ acquires great importance only at low temperatures, typically below 1 K in ^4He , and is relevant to turbulence decay experiments. At higher temperatures friction damps Kelvin waves, smoothing vortex lines and dissipating superfluid energy. Here we shall describe only the basic ideas, avoiding the most debated details.

Neglecting the interaction between separate vortex lines (besides the small regions around vortex reconnection events, which will be discussed later), at $k\ell \gg 1$ superfluid turbulence can be considered as a system of Kelvin waves with different wavevectors interacting with each other on the same vortex. The prediction that this interaction results in turbulent energy transfer toward large k [63] was confirmed by numerical simulations in which energy was pumped into Kelvin waves at intervortex scales by vortex reconnections [64] or simply by exciting the vortex lines [65]. The first analytical theory of Kelvin wave turbulence (propagating along a straight vortex line and in the limit of small amplitude compared to wavelength) was proposed by Kozik and Svistunov [66] (KS), who showed that the leading interaction is a six-wave scattering process (three incoming waves and three outgoing waves). Under the additional assumption of locality of the interaction (that only compatible wave-vectors contribute to most of the energy transfer) KS found that (using the same normalisation of other hydrodynamic spectra such as Eqs. [3]) the energy spectrum of Kelvin waves is

$E_{\text{KW}}^{\text{KS}}(k) = C_{\text{KS}} \Lambda \varepsilon_{\text{KW}}^{1/5} k^{7/5} \ell^{-8/5} k^{-7/5}$, $C_{\text{KS}} \sim 1$, (KS spectrum). Here $\Lambda \equiv \ln(\ell/\xi) \simeq 12$ or 15 in typical ^4He and ^3He experiments, and ε_{KW} is the energy flux in three dimensional \mathbf{k} -space.

Later L’vov-Nazarenko (LN) [67] criticised the KS assumption of locality and concluded that the leading contribution to the energy transfer comes from a six waves scattering in which two wave vectors (from the same side) have wavenumbers of the order of $1/\ell$. LN concluded that the spectrum is

$$E_{\text{KW}}^{\text{LN}}(k) = C_{\text{LN}} \frac{\Lambda \varepsilon_{\text{KW}}^{1/3}}{\Psi^{3/2} k^{5/3}}, \quad \Psi = \frac{4\pi E_{\text{KW}}}{\Lambda k^2}, \quad (\text{LN spectrum}),$$

where analytically found $C_{\text{LN}} \approx 0.304$ [93].

This KS vs LN controversy triggered an intensive debate (see e.g. Refs [68, 69, 70, 71, 72, 73]), which is outside the scope of this article. We only mention that the three-dimensional energy spectrum $E_{\text{KW}}(k)$ can be related to the one-dimensional amplitude spectrum

$A_{\text{KW}}(k)$ by $E_{\text{KW}}(k) \sim \hbar \omega(k) n(k)$ where $\omega(k) \propto k^2$ is the angular frequency of a Kelvin wave of wavenumber k , $\hbar \omega(k)$ the energy of one quantum, and $n(k) \sim A_{\text{KW}}(k)$ the number of quanta; therefore, in terms of the Kelvin waves amplitude spectrum (which is often reported in the literature and can be numerically computed), the two predictions are respectively $A_{\text{KW}}^{\text{KS}} \sim k^{-17/5} = k^{-3.40}$ (KS) and $A_{\text{KW}}^{\text{LN}} \sim k^{-11/3} = k^{-3.67}$ (LN).

The two predicted exponents (-3.40 and -3.67) are very close to each other; indeed VFM simulations [74] could not distinguish them (probably because the numerics were not in the sufficiently weak regime of the theory in terms of ratio of amplitude to wavelength). Nevertheless, more recent GPE simulations by Krstulovic [75] based on long time integration of Eq. [7] and averaged over initial conditions (slightly deviating from a straight line) support the LN spectrum. The most recent VFM simulations by Baggaley and Laurie [76] observe a remarkable agreement with the LN spectrum with $C_{\text{LN}}^{\text{num}} \approx 0.308$ close to $C_{\text{LN}}^{\text{anal}} \approx 0.304$ while $C_{\text{KS}}^{\text{num}} \approx 0.009$ differs from the KS-estimate $C_{\text{KS}} \sim 1$.

At finite temperature, it was shown in Ref. [77] that the Kelvin wave spectrum is suppressed by mutual friction for $k > k_*$, reaching core scale ($k_* \xi \approx 1$) at $T \simeq 0.07$ K and fully disappears at $T \simeq 1$ K, when $k_* \ell \approx 1$.

6C. Intermediate regimes. The regions of the spectrum just below and above the intervortex scale $k\ell \simeq 1$ is difficult, because both eddy-type motions and Kelvin waves are important, and the discreteness of the superfluid vorticity prevents direct application of the tools of classical hydrodynamics. Nevertheless, some attempts have been made to understand the physics of these spectral regions.

At $T > 0$, direct numerical simulations of the truncated HVBK model for $1\text{K} < T < T_\lambda$ confirmed the KO–41 scaling of the two locked fluids at large scales (see Fig. 2A). At smaller scales $k > k_{\text{meso}}$, an intermediate (meso) regime appeared that expands as T is lowered [56]. Apparently, superfluid energy, cascading from larger length scales, accumulates beyond k_{meso} . At the lowest temperatures, this energy appears to thermalize, approaching equipartition with $E_s(k) \propto k^2$, as shown by the red curve of Fig. 2A. The process saturates when the friction coupling with the normal fluid becomes strong enough to balance the incoming energy flux $\varepsilon(k_{\text{meso}})$. In physical space, this mesoscale thermalization should manifest itself as a randomisation of the vortex tangle. The effect is found to be strongly temperature dependent [81]: $k_{\text{meso}} \propto k_\ell \sqrt{\rho_n/\rho}$. Such accumulation of thermalized superfluid excitations at small scales and finite temperature was predicted by an earlier model developed to interpret vortex line density spectra [53].

At $T = 0$, comparison [4] of the hydrodynamic spectrum [3] with the LN Kelvin wave spectrum at $T = 0$ suggests that the one dimensional nonlinear transfer mechanisms among weakly nonlinear Kelvin waves on individual vortex lines is less efficient than the three-dimensional, strongly nonlinear eddy-eddy energy transfer. The consequence is an energy cascade stagnation at the crossover between the collective eddy-dominated scales and the single vortex wave-dominated scales. The total energy flux, $\varepsilon(k)$ arising from hydrodynamic and Kelvin-wave contributions, was modelled [92] by dimensional reasoning in the differential approximation, similar to Eq. [4]: for $k \rightarrow 0$ the energy flux is purely hydrodynamic and $E(k)$ is given by Eq. [5], while for $k \rightarrow \infty$ it is purely supported by Kelvin waves and $E(k)$ is the LN Kelvin wave spectrum. This approach leads to the ordinary differential equation $\varepsilon(k) = \text{constant}$, which was solved numerically. The predicted energy spectra $E(k)$ for different values of Λ , shown in Fig. 2C, exhibit a bottleneck energy accumulation $E(k) \propto k^2$ in agreement with Eq. [5].

Finally, there have been attempts to go beyond KO–41 and address the problem of intermittency. The first numerical study of intermittent exponents [90] did not find any intermittent effect peculiar to superfluid turbulence neither at low temperature ($T \simeq 0.5T_\lambda$, $\rho_s/\rho_n = 40$) nor at and high temperature ($T \simeq 0.99T_\lambda$, $\rho_s/\rho_n =$

0.1), in agreement with experiments [17, 90], all performed on the low temperature side ($T \lesssim 0.7T_\lambda$, $\rho_s/\rho_n > 5.7$).

Recently, the intermediate temperature corresponding to $\rho_s \approx \rho_n$ has been explored with shell model simulations [60] with eight decades of k -space, which allowed detailed comparison of classical and superfluid turbulent statistics. It was found that for T slightly below T_λ , when $\rho_s/\rho_n \ll 1$, the statistics of turbulent superfluid ^4He appeared similar to that of classical fluids, because the superfluid component can be neglected (green lines in Fig. 6 in the Appendix). The same result applies to $T \ll T_\lambda$ ($\rho_n \ll \rho_s$), as expected due to the inconsequential role played by the normal component (blue lines in Fig. 6). A difference between classical and superfluid intermittent behaviour in a wide (up to three decades) interval of scales appeared in the range $0.8T_\lambda < T < 0.9T_\lambda$ ($\rho_s \approx \rho_n$) – red lines in Fig. 6. The exponents of higher order correlation functions also deviate further from the KO–41 values.

7. Outlook.

We conclude that, at large hydrodynamic scales $k_D \ll k \ll k_\ell$, the evidence for the KO–41 $k^{-5/3}$ scaling of the superfluid energy spectrum which arises from experiments, numerical simulations and theory (across all models used) is strong and consistent, and appears to be independent of temperature (including the limit of zero temperature in the absence of the normal fluid [38, 39, 51, 12]). This direct spectral evidence is also fully consistent with an indirect body of evidence arising from measurements of the kinetic energy dissipation ([84, 85, 86, 87, 22]) and vortex line density decay [88, 89] in turbulent helium flows. The main open issue is the existence of vortex bundles [12, 15] predicted by the VFM, for which there is no direct experimental observation yet. Intermittency effects, predicted by shell models [60], also await experimental evidence.

At the quantum length scales ($k \gg k_\ell$) the situation is less clear. This regime is very important at the lowest temperatures, where, in the absence of friction, the Kelvin waves are not damped, and energy is transferred downscale until the waves are short and fast that it is radiated away. In the weak regime (small Kelvin wave amplitudes compared to wavelength) the proposed KS and LN Kelvin wave energy spectra differ on principles, but their actual numerical difference is small; this has encouraged the development of better numerics, and the most recent GPE and VFM simulations favour the LN scenario. Unfortunately there is not yet any direct experimental observation of the energy spectrum at such length scales.

What happens at intermediate length scales ($k\ell \approx 1$) is even less understood. The truncated HVBK model (at finite T), predicts a temperature–dependent upturning of the spectrum in this region of k -space. If confirmed by the experiments and the VFM model, this would signify the striking appearance of quantum effects at scales larger than ℓ . Further insight could arise from better understanding of fluctuations of the vortex line density. It is worth noticing that similar macroscopic manifestation of the singular nature of the superfluid vorticity was also predicted for the pressure spectrum [82]. In the $T \rightarrow 0$ limit, the eddy–dominated, three–dimensional Kolmogorov cascade at $R \gg \ell$ should merge into the one–dimensional Kelvin wave cascade at $R \ll \ell$ on individual vortex lines. The differential model [92] predicts bottleneck accumulation of energy in the cross–over region at $k\ell \approx 1$ between the two cascades, that explains experimentally observed [94] drop in about 30 times in the effective (Vinen’s) viscosity ν' . However the bottleneck has not been directly observed in the experiments yet and lacks the confirmation of the VFM. A related open issue is the role of vortex reconnections in the strong regime of the cascade (large Kelvin wave amplitudes compared to wavelength).

Experimentally, the limited resolution of the anemometer is responsible for the cut-off at high frequency/small scale. Thus, the observed spectra reveal only the integral scales and the upper half of the inertial scales. To circumvent this limitation, a first approach is to scale up the experiment (at given Reynolds number Re_κ) so that all characteristic flow scales are magnified and better resolved with existing probes. This approach has been undertaken with the construction of a 78-cm diameter He-II Von Karman flow in Grenoble [19] that is one order of magnitude larger than the 1998’s reference cell. Another approach is to scale down the probes. For practical reasons it is difficult to miniaturise much further stagnation pressure probes without a significant decrease of their sensibility or time response. New types of anemometers need to be invented. One possibility arises from the recent development of fully micro-machined anemometers based on the deflection of a silicon cantilever (see the bottom left sketch of Fig. 4). Preliminary spectral measurements with a resolution of $100\mu\text{m}$ have been recently reported in a He-II test facility [91].

ACKNOWLEDGMENTS. C.F.B is grateful to Y.A. Sergeev for discussions and to EPSRC for financial support (grant number EP/I019413/1). P.-E.R. acknowledges numerous discussions with E. Lévêque and financial support from ANR-09-BLAN-0094 and from la Région Rhône-Alpes.

1. A.F. Annett (2004) *Superconductivity, superfluids and condensates* (Oxford University Press, Oxford).
2. L. Skrbek and K.R. Sreenivasan (2012), *Developed quantum turbulence and its decay*, Phys. Fluids (24): 011301.
3. C.F. Barenghi, S. Hulton and D.C. Samuels (2002), *Polarization of superfluid turbulence*, Phys. Rev. Lett. (89): 275301.
4. V. S. L’vov, S. V. Nazarenko, O. Rudenko (2007), *Bottleneck crossover between classical and quantum superfluid turbulence*, Phys. Rev. B 76, 024520.
5. A.W. Baggaley, J. Laurie, and C.F. Barenghi (2012), *Vortex-density fluctuations, energy spectra, and vortical regions in superfluid turbulence*, Phys. Rev. Lett. (109): 205304.
6. R.J. Donnelly (1991) *Quantised Vortices In Helium II* (Cambridge University Press, Cambridge, UK).
7. C.F. Barenghi, R.J. Donnelly, and W.F. Vinen (1982), *Friction on quantized vortices in helium II* J. Low Temp. Phys. (52): 189–247.
8. U. Frisch (1995), *Turbulence. The legacy of A.N. Kolmogorov* (Cambridge University press, Cambridge, UK).
9. K. P. Zysin and V. A. Sirota (2013) *Multifractal structure of fully developed turbulence*, Phys. Rev. E 88, 043017
10. C. Leith (1967), *Diffusion approximation to inertial energy transfer in isotropic turbulence*, Phys. Fluids (10): 1409–1416.
11. C. Connaughton and S. Nazarenko (2004), *Warm Cascades and Anomalous Scaling in a Diffusion Model of Turbulence*, Phys. Rev. Lett. (92): 044501.
12. A.W. Baggaley, C.F. Barenghi, A. Shukurov, and Y.A. Sergeev (2012), *Coherent vortex structures in quantum turbulence*, Europhys. Lett. (98): 26002.
13. W.F. Vinen (2001), *Decay of superfluid turbulence at very low temperature: the radiation of sound from a Kelvin wave on a quantized vortex*, Phys. Rev. B (64): 134520.
14. S.N. Fisher (2008), *Turbulence experiments in superfluid ^3He at very low temperatures*, in *Vortices and Turbulence at Very Low Temperatures*, edited by C.F. Barenghi and Y.A. Sergeev, CISM Courses and Lectures, vol. 501, Springer Verlag (2008), 157–257.
15. A.W. Baggaley, L.K. Sherwin, C.F. Barenghi, and Y.A. Sergeev (2012), *Thermally and mechanically driven quantum turbulence in helium II*, Phys. Rev. B (86): 104501.
16. S. K. Nemirovskii (2013), *Quantum turbulence: Theoretical and numerical problems* Physics Reports, (524): 85–120.
17. J. Maurer, and P. Tabeling (1998), *Local investigation of superfluid turbulence*, Europhys. Lett. (43): 29–34.
18. D. Schmoranzler, M. Rotter, J. Sebek, and L. Skrbek (2009), *Experimental setup for probing a von Karman type flow of normal and superfluid helium*, Experimental Fluid Mechanics 2009, Proceedings of the International Conference, 304
19. <http://www.euhit.org/infrastructures/ghi>,
20. J. Salort, B. Chabaud, Lévêque E. and P.-E. Roche (2012), *Energy cascade and the four-fifths law in superfluid turbulence*, Europhys. Lett. (97): 34006.
21. P.E. Roche, P. Diribarne, T. Didelot, O. Francais, L. Rousseau, and H. Willaime (2007), *Vortex density spectrum of quantum turbulence*, Europhys. Lett. (77): 66002.
22. J. Salort J, et al. (2010), *Turbulent velocity spectra in superfluid flows*, Phys. Fluids (22): 125102.
23. S.A. Vitiello, L. Reatto, G.V. Chester, and M.H. Kalos (1996), *Vortex line in superfluid ^4He : A variational Monte Carlo calculation*, Phys. Rev. B (54): 1205–1212.

24. Y Pomeau, and S Rica (1993), *Model of super flow with rotons*, Phys. Rev. Lett. (71):247–250.
25. K.W. Schwarz (1988), *Three-dimensional vortex dynamics in superfluid 4He: Homogeneous superfluid turbulence*, Phys. Rev. B (38): 2398–2417.
26. P.G. Saffman (1992), *Vortex Dynamics* (Cambridge University Press, Cambridge, UK).
27. R.J. Donnelly and C.F. Barenghi (1998), *The observed properties of liquid helium at the saturated vapor pressure*, J. Phys. Chem. (6): 1217–1274.
28. A.W. Baggaley and C.F. Barenghi (2012), *Tree method for quantum vortex dynamics*, J. Low Temp. Phys. (66): 3–20.
29. A.W. Baggaley (2012), *The sensitivity of the vortex filament method to different reconnections models*, J. Low Temp. Phys. (68): 18.
30. S. Zuccher, M. Caliari, and C.F. Barenghi (2012), *Quantum vortex reconnections*, Phys. Fluids (24): 125108.
31. D. Kivotides, C.F. Barenghi, and D.C. Samuels (2000), *Triple vortex ring structure in superfluid helium II*, Science (290): 777–779.
32. D. Kivotides (2011), *Spreading of superfluid vorticity clouds in normal-fluid turbulence*, J. Fluid Mech. (668): 58–75.
33. H.E. Hall and W.F. Vinen (1956), *The rotation of liquid helium II. II. The theory of mutual friction in uniformly rotating helium II*, Proc. Roy. Soc. London A (238): 215–234.
34. R.N. Hills and P.H. Roberts (1977), *Superfluid mechanics for a high density of vortex lines*, Arch. Rat. Mech. Anal. (66): 43–71.
35. C.F. Barenghi (1992), *Vortices and the Couette flow of helium II*, Phys. Rev. B (45): 2290–2293.
36. K.L. Henderson, C.F. Barenghi and C.A. Jones (1995), *Nonlinear Taylor Couette flow of helium II*, J. Fluid Mech. (283): 329–340.
37. J.J. Hosio, V.B. Eltsov, R. de Graaf, P.J. Heikkinen, R. Hänninen, M. Krusius, V.S. L'vov and G.E. Volovik, *Superfluid vortex front at $T \rightarrow 0$: decoupling from the reference frame*, Phys. Rev. Lett. (107): 135302 (2011).
38. C. Nore, M. Abid, and M.E. Brachet (1997), *Kolmogorov turbulence in low temperature superflows*, Phys. Rev. Lett. (78): 3896–3899.
39. M. Kobayashi, and M. Tsubota (2005), *Kolmogorov spectrum of superfluid turbulence: numerical analysis of the Gross-Pitaevskii equation with a small-scale dissipation*, Phys. Rev. Lett. (94): 065302.
40. N. Sasa, T. Kano, M. Machida, V. S. L'vov, O. Rudenko and M. Tsubota (2011), *Energy spectra of quantum turbulence: Large-scale simulation and modelling*, Phys. Rev. B (84): 054525.
41. M. Tsubota and M. Kobayashi (2009), *Energy spectra of quantum turbulence*, in *Progress of Low Temperature Physics*, 1–43, ed. by M. Tsubota and W.P. Halperin, Elsevier.
42. N. P. Proukakis and B. Jackson (2008), *Finite-temperature models of Bose-Einstein condensation*, J Phys B-At Mol Opt 41 (2008): 203002.
43. M. E. Brachet (2012), *Gross-Pitaevskii description of superfluid dynamics at finite temperature: A short review of recent results*, C. R. Physique (13): 954.
44. G. Krstulovic and M. Brachet (2011), *Anomalous vortex-ring velocities induced by thermally excited Kelvin waves and counterflow effects in superfluids*, Phys. Rev. B (83): 132506.
45. A.J. Allen, E. Zaremba, C.F. Barenghi, and N.P. Proukakis (2013), *Observable vortex properties in finite-temperature Bose gases* Phys. Rev. A (87): 013630.
46. R.G.K.M. Aarts, and A.T.A.M. de Waele (1994), *Numerical investigation of the flow properties of He II*, Phys. Rev. B (50) 10069–10079.
47. D. Kivotides, C.J. Vassilicos, D.C. Samuels, and C.F. Barenghi (2002), *Velocity spectra of superfluid turbulence*, Europhys. Lett. (57): 845–851.
48. D.R. Osborne, J.C. Vassilicos, K. Sung, and J.D. Haigh (2006), *Fundamentals of pair diffusion in kinematic simulations of turbulence*, Phys. Rev. E (74): 036309.
49. K. Morris, J. Koplik, and D.W.I. Rouson (2008), *Vortex locking in direct numerical simulations of quantum turbulence*, Phys. Rev. Lett. (101): 015301.
50. D. Kivotides (2006), *Coherent structure formation in turbulent thermal superfluids*, Phys. Rev. Lett. (96): 175301.
51. T. Araki, M. Tsubota, and S.K. Nemirovskii (2002), *Energy Spectrum of Superfluid Turbulence with No Normal-Fluid Component*, Phys. Rev. Lett. (89): 145301.
52. H. Adachi, S. Fujiyama, and M. Tsubota (2010), *Steady state counterflow turbulence: simulation of vortex filaments using the full Biot-Savart law*, Phys. Rev. B (81): 104511.
53. P.E. Roche, and C.F. Barenghi (2008), *Vortex spectrum in superfluid turbulence: interpretation of a recent experiment*, Europhys. Lett. (81): 36002.
54. L. Merahi, P. Sagaut, and Z. Abidat (2006), *A closed differential model for large-scale motion in HVBK fluids*, Europhys. Lett. (75): 757.
55. P.-E. Roche, C. F. Barenghi, and E. Lévêque (2009), *Quantum turbulence at finite temperature: the two-fluids cascade*, Europhys. Lett. (87): 54006.
56. J. Salort, P.-E. Roche and E. Lévêque (2011), *Mesoscale Equipartition of kinetic energy in Quantum Turbulence*, Europhys. Lett. (94): 24001.
57. J. Tchoufag and P. Sagaut (2010), *Eddy damped quasi normal Markovian simulations of superfluid turbulence in helium II*, Phys. Fluids, (22): 125103.
58. D. H. Wacks and C. F. Barenghi (2011), *Shell model of superfluid turbulence*, Phys. Rev. B (84): 184505.
59. L. Boué, V. L'vov, A. Pomyalov, and I. Procaccia (2012), *Energy spectra of superfluid turbulence in ^3He* Phys. Rev. B (85): 104502.
60. L. Boué, V. L'vov, A. Pomyalov, and I. Procaccia (2013), *Enhancement of intermittency in superfluid turbulence*, Phys. Rev. Lett. (110): 014502.
61. V. S. L'vov, S. V. Nazarenko, G. E. Volovik (2004), *Energy spectra of developed superfluid turbulence*, JETP Letters (80) 479.
62. V. S. L'vov, S. V. Nazarenko, L. Skrbek (2006), *Energy Spectra of Developed Turbulence in Helium Superfluids*, J. Low Temp. Phys. (145): 125.
63. B. V. Svistunov (1995), *Superfluid turbulence in the low-temperature limit*, Phys. Rev. B (52): 3647.
64. D. Kivotides, J.C. Vassilicos, D.C. Samuels, and C.F. Barenghi (2001), *Kelvin Waves Cascade in Superfluid Turbulence*, Phys. Rev. Lett. (86): 3080.
65. W. F. Vinen, M. Tsubota, and A. Mitani (2003), *Kelvin-Wave Cascade on a Vortex in Superfluid 4He at a Very Low Temperature*, Phys. Rev. Lett. (91): 135301.
66. E. Kozik, B.V. Svistunov (2004), *Kelvin-wave cascade and decay of superfluid turbulence*, Phys. Rev. Lett. (92): 035301.
67. V.S. L'vov, S. Nazarenko (2010), *Spectrum of Kelvin-wave turbulence in superfluids* Pisma v ZhETFf (91): 464.
68. J. Laurie, V.S. L'vov, S. Nazarenko, O. Rudenko (2010), *Interaction of Kelvin waves and nonlocality of energy transfer in superfluids*, Phys. Rev. B. (81): 104526.
69. V.V. Lebedev, V.S. L'vov (2010), *Symmetries and interaction coefficient of Kelvin waves* J. Low Temp. Phys. (161): 548–554.
70. V.V. Lebedev, V.S. L'vov, S.V. Nazarenko (2010), *Reply: On role of symmetries in Kelvin wave turbulence* J. Low Temp. Phys. (161): 606–610.
71. E. Kozik, B.V. Svistunov (2010), *Geometric symmetries in superfluid vortex dynamics*, Phys. Rev. B (82):(R) 140510.
72. E.B. Sonin (2012), *Symmetry of Kelvin-wave dynamics and the Kelvin-wave cascade in the $T=0$ superfluid turbulence*, Phys. Rev. B (85): 104516 and *Reply to comment*, Phys. Rev. B (86), 226502.
73. V.S. L'vov, S.V. Nazarenko (2012), *Comment on Symmetry of Kelvin-wave dynamics and the Kelvin-wave cascade in the $T=0$ superfluid turbulence*, Phys. Rev. B (86): 226501
74. A.W. Baggaley and C.F. Barenghi (2011), *Spectrum of turbulent Kelvin-waves cascade in superfluid helium*, Phys. Rev. B (83): 134509.
75. G. Krstulovic (2012), *Kelvin-wave cascade and dissipation in low-temperature superfluid vortices* Phys. Rev. E (86): 055301.
76. A.W. Baggaley and J. Laurie (2013), *The Kelvin-wave cascade in the vortex filament model*. arXiv:1204.4034v4.
77. L. Boué, V. L'vov, and I. Procaccia (2012), *Temperature suppression of Kelvin-wave turbulence in superfluids*, Europhys. Lett. (99): 46003.
78. Y. Minoda, M. Tsubota, and W. Vinen (2012), *Decay of counterflow quantum turbulence in superfluid 4He*, J. Low Temp. Phys. 1 10.1007/s10909-012-0800-7
79. D. C. Samuels and D. Kivotides (1999), *A damping length scale for superfluid turbulence* Phys. Rev. Lett. (83): 5306.
80. W. F. Vinen and J. J. Niemela (2002), *Quantum turbulence*, J. Low Temp. Phys. (128): 167.
81. P.-E. Roche (2013), *Energy spectra and characteristic scales of quantum turbulence investigated by numerical simulations of the two-fluid model*, To appear in the Proc. of the 14th EUROMECH European Turbulence Conference, Sept 1-4, 2013, Lyon.
82. D. Kivotides, J.C. Vassilicos, C.F. Barenghi, M.A.I. Khan, and D.C. Samuels (2001), *Quantum signature of superfluid turbulence* Phys. Rev. Lett. (87): 275302.
83. L.K. Sherwin, A.W. Baggaley and C.F. Barenghi, *in preparation*
84. P. Walstrom, J. Weisend, J. Maddocks, and S. Van Sciver (1988) *Turbulent flow pressure drop in various He II transfer system components*. Cryogenics (28):101
85. B. Roussel, G. Claudet, A. Gauthier, P. Seyfert, A. Martinez, P. Lebrun, M. Marquet, and R. van Weelderden (1994) *Pressure drop and transient heat transport in forced flow single phase helium II at high Reynolds numbers*. Cryogenics (34):317
86. M. Abid, M. E. Brachet, J. Maurer, C. Nore, and P. Tabeling (1998) *Experimental and numerical investigations of low-temperature superfluid turbulence* Eur. J. Mech B-Fluid (17):665
87. S. Fuzier, B. Baudouy, and S. W. Van Sciver (2001) *Steady-state pressure drop and heat transfer in He II forced flow at high Reynolds number* Cryogenics (41):453
88. L. Skrbek, J. J. Niemela, and K. R. Sreenivasan (2001) *Energy spectrum of grid-generated Hell turbulence* Phys. Rev. E, (64):067301
89. J. Niemela, K. Sreenivasan, and R. Donnelly (2005) *Grid generated turbulence in helium II* J. Low Temp. Phys. (138):537
90. J. Salort, B. Chabaud, E. Lévêque, and P.-E. Roche (2011). *Investigation of intermittency in superfluid turbulence*. In *J. Phys.: Conf. Ser.*, volume 318 of *Proceedings of the 13th EUROMECH European Turbulence Conference, Sept 12-15, 2011, Warsaw*, page 042014. IOP Publishing.
91. J. Salort, A. Monfardini, and P.-E. Roche (2012), *Cantilever anemometer based on a superconducting micro-resonator: Application to superfluid turbulence*, Rev. Sci. Instrum. (83): 125002.
92. V. S. L'vov, S. V. Nazarenko, O. Rudenko (2008), *Gradual eddy-wave crossover in superfluid turbulence*, J. Low Temp. Phys. (153): 140–161.
93. L. Boué, R. Dasgupta, J. Laurie, V.S. L'vov, S. Nazarenko, and I. Procaccia, (2011) *Exact solution for the energy spectrum of Kelvin-wave turbulence in superfluids*, Phys. Rev. B, 84, 064516.
94. P. M. Walmsley, A. I. Golov, H. E. Hall, A. A. Levchenko, and W. F. Vinen, *Dissipation of Quantum Turbulence in the Zero Temperature Limit*, Phys. Rev. Letts, 99, 265302 (2007).

Appendix

APPENDIX

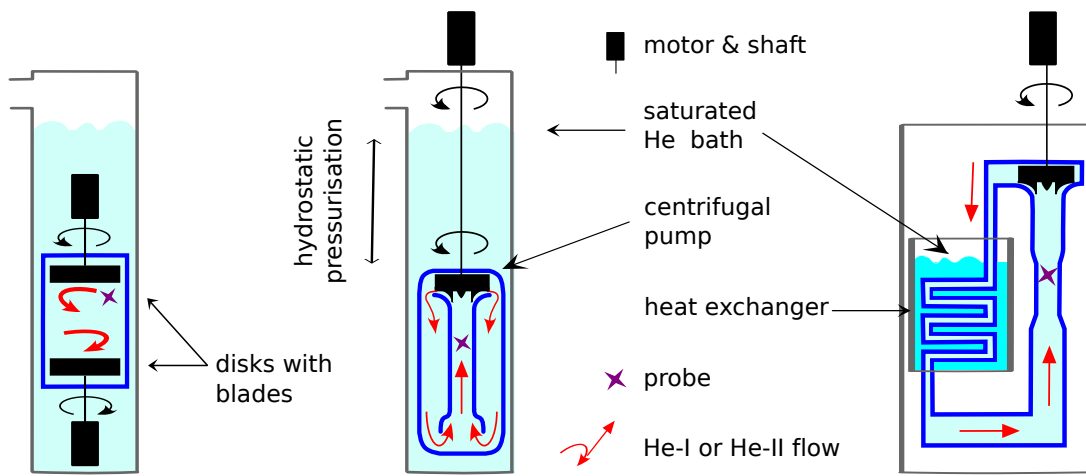


Fig. 3: From left to right: Von Karman flows ([17, 18, 19]), wind-tunnels ([20, 21]) and pressurised circulator cooled through a heat exchanger ([22]).

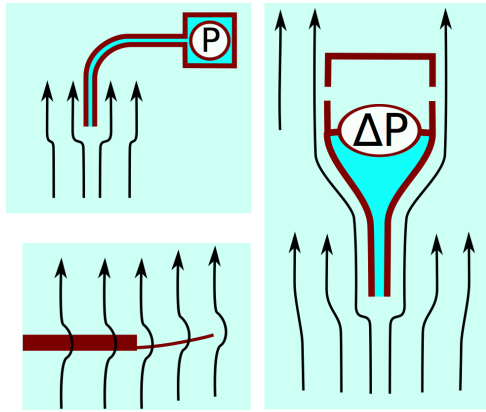


Fig. 4: Stagnation pressure velocity probes without static pressure reference (top-left) ([17, 22]), stagnation pressure velocity probe with a static pressure reference (right) ([22, 20]), and cantilever-based velocity probe (bottom left) [91]. In the arrangement depicted at the right, the use of a differential pressure probe allows to remove the “static” pressure variation of the flow associated with turbulent pressure fluctuations and acoustical background noise.

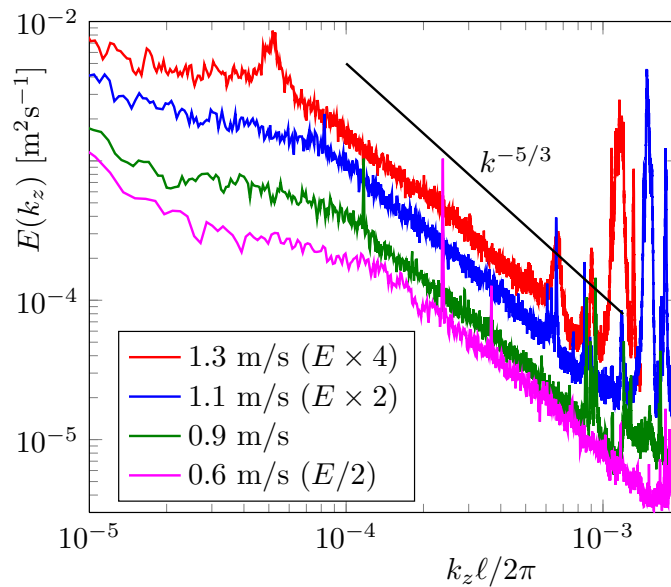


Fig. 5: Energy spectra for different mean flow velocities for $T = 1.55\text{K}$ in the superfluid wind-tunnel presented in [20]. An arbitrary vertical offset had been introduced for clarity (see legend). For a compensated plot, see [21]

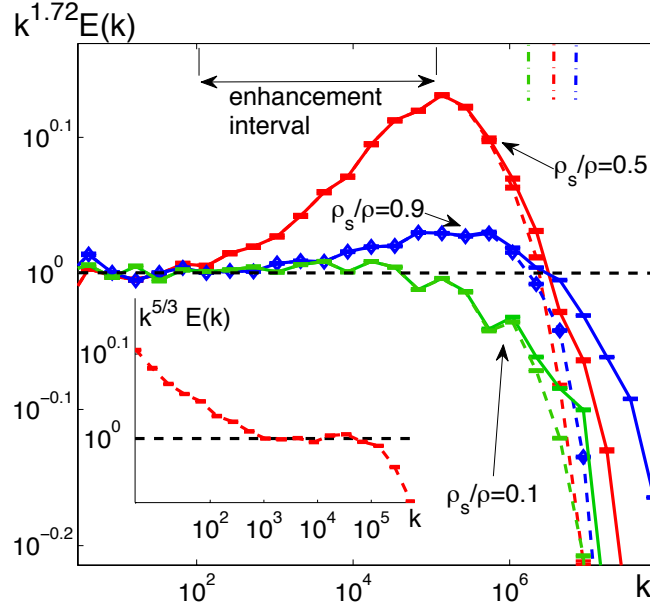


Fig. 6: Superfluid (solid lines) and normal fluid (dashed lines) compensated energy spectra $k^{1.72}E(k)$; the compensation factor is the classical energy spectrum with intermittency correction. Inset: $k^{5/3}E(k)$ for $T = 0.9 T_\lambda$. Shell model simulation of the HVBK model at $T/T_\lambda = 0.99$ K (green), 0.9 (red) and 0.9 (blue), corresponding to $\rho_s/\rho = 0.1, 0.5$, and 0.9 respectively Ref. [60]. The vertical dash lines indicate $k\ell \equiv 1/\ell$.

Appendix section : Superfluid turbulence in ^3He

In Sec. 6A we discuss large scale $R \gg \ell$ turbulent motions of normal and superfluid components in ^4He on the ground of the HVBK Eqs. [9]. Noticing that the kinematic viscosity of normal-fluid component in ^3He is so large that, in all ^3He turbulence experiments, we expect the normal fluid to be at rest ($\mathbf{u}_n = 0$) with respect to the walls of the container. Liquid ^3He thus provides us with a simpler turbulence problem (superfluid turbulence in the presence of linear friction against a stationary normal fluid) than ^4He (superfluid turbulence in the presence of normal fluid turbulence).

With $\mathbf{u}_n = 0$ we have to skip Eq. [10b] in our paper and to put $E_{ns} = 0$ in Eq. [10a]. Using the differential approximation Eq. [4] for the energy spectrum, the continuity Eq. [10a] in the stationary case becomes

$$\frac{1}{8} \frac{d}{dk} \left[\sqrt{k^{11} E_s(k)} \frac{d}{dk} \frac{E_s(k)}{k^2} \right] + \Gamma E_s(k) = 0.$$

Analytical solutions of this equation found and analyzed in [59, 61] are in good agreement with the results of numerical simulation of the shell model to the HVBK Eqs. [9], providing us with quasi-qualitative description of turbulent energy spectra in ^3He over a wide region of temperatures and wave vectors.